# Backstepping-Based DPC Strategy of a Wind Turbine-Driven DFIG Under Normal and Harmonic Grid Voltage

Pinghua Xiong and Dan Sun, *Member, IEEE*

***Abstract*—This paper presents a sort of nonlinear backstepping-based algorithm combining with direct power control (DPC) to a wind turbine-driven doubly fed induction generator (DFIG) under normal and especially harmonic grid voltage. First, the power control objectives are analyzed and designed under normal and harmonic grid voltage for the purpose of harmonic stator current suppression; second, a unified mathematic model of a DFIG under normal and harmonic grid voltage is founded, exploring its power model in detail; finally, the backstepping algorithm is introduced briefly and the backstepping-based DPC (BS-DPC) algorithm of the DFIG is developed under normal and harmonic grid voltage. The comparative simulation results between vector control (VC) with resonant controller, look-up table DPC (LUT-DPC) and BS-DPC under normal grid voltage verify that the proposed BS-DPC realizes the decoupling control of active and reactive power of DFIG, with better dynamic performance than VC, as well as with better steady performance than LUT-DPC. Under the harmonic grid voltage, further simulation results verify the effectiveness of BS-DPC for suppressing the harmonic stator current of the DFIG in contrast to VC with a resonant controller and LUT-DPC with improved control objectives proposed by this paper; meanwhile, the adaptability of BS-DPC to minute frequency derivation, harmonic component order and distorted degree of the grid voltage under harmonic conditions are verified as well.**

***Index Terms*—Backstepping-based direct power control (BS-DPC), doubly fed induction generator (DFIG), grid voltage frequency adaptability, harmonic order adaptability, harmonic stator current suppression, normal grid voltage.**

## NOMENCLATURE

| | |
|---|---|
| $\boldsymbol{U}_{\boldsymbol{S\alpha\beta}}$, $V_{r\boldsymbol{\alpha}\beta}$ | Stator, rotor voltage vectors. |
| $I_{\boldsymbol{S\alpha\beta}}$, $I_{r\boldsymbol{\alpha}\beta}$ | Stator, rotor current vectors. |
| $P_{\boldsymbol{S}}$, $Q_{\boldsymbol{S}}$ | Stator output active and reactive powers. |
| $\boldsymbol{S}$ | Apparent power |
| $L_S$, $L_r$ | Stator, rotor self-inductances. |
| $L_m$ | Mutual inductance. |
| $R_S$, $R_r$ | Stator, rotor resistances. |
| $\omega$ | Angular frequency |
| Subscripts | |
| *A*, *B*, *C* | Stator A, B, and C phase |
| *a*, *b*, *c* | Rotor a, b, and c phase |
| $\alpha$, $\beta$ | Two phase stationary coordinate. |
| *S*, *r* | Stator, rotor. |
| *wlip* | Sliding difference |
| *_f*, *_ h*, | Fundamental, harmonic frequency |
| *_ main*, *_ comp*, | Main, compensation control |
| * | Reference value. |
| ^ | Conjugated vector. |

Manuscript received April 7, 2015; accepted August 27, 2015. Date of publication September 9, 2015; date of current version January 7, 2016. This work was supported in part by the Zhejiang Provincial Natural Science Foundation of China (LY13E070001) and the National Natural Science Foundation of China (51377141). Recommended for publication by Associate Editor M. Molinas. *(Corresponding author: Dan Sun).*

The authors are with the College of Electrical Engineering, Zhejiang University, Hangzhou 310027, China (e-mail: 21310144@zju.edu.cn; sundan@zju.edu.cn).

Digital Object Identifier 10.1109/TPEL.2015.2477442

## I. INTRODUCTION

REALIZING the value of natural resources and environmental problems caused by the emissions, many nations around the world have been making many researches and efforts to introduce more clean energies into their power grid to share in the role played by the traditional power generations based on fossil fuel which are considered to be unsustainable in a long term. In the last decades, except for hydropower, the wind power gained a growth more significant than any other renewable energy in many nations, and at present, it has been playing an important part in the modern energy supply system rather than an ancillary. So far, among various configuration of wind-driven generators, the doubly fed induction generator (DFIG) equipped with a partial-scale power converter has been dominating on the market due to its edges of variable speed constant frequency operation, low converter costs, and low-power losses, etc. However, for the two causes that the DFIG's stator is directly connected to the grid via step-up transformers and relative to the total generated power, the power capacity of the grid-side and rotor-side converters are limited, the DFIG generation system tends to be very sensitive to any grid disturbances. Meanwhile, with the number of nonlinear and single-phase loads increasing more and more, the amount and sort of harmonics in the power grid are growing. Harmonics can cause serious problems or even damages of electrical or electronics devices including DFIG; on the other hand, there are many standards and documents [1]–[4] ruling that a certain degree of harmonic voltage components be permitted to exist, DFIGs should keep in being connected to the grid under this situation for the roles in the grid the wind power has played, and the harmonic current poured by them into the grid should be lower than a certain level. Therefore, a lot of methods for elimination of harmonics distortion in the power system are developed and implemented.

According to [5], the active and reactive power produced by DFIG encompasses alternative components unavoidably under the distorted grid voltage; in traditional vector control (VC), the control strategy was carried out in the synchronous reference frame, leading to alternating components of multiple times

fundamental frequency in the controlled rotor current. Although high performance could be achieved by the proportional integral (PI) controller with the direct variables, the effectiveness will deteriorate significantly under alternating variables for its limited bandwidth and gain margin. Therefore, the operating performance of present prevailing VC and direct power control (DPC) strategy [6] of the DFIG which adopt the PI controller normally would be impacted considerably under harmonic grid voltage situation.

For the purpose of solving difficulty of the regulating of alternating variables under the harmonic grid voltage, Ramos *et al.* [7] proposed a harmonic stator current compensation method under the multiple synchronous rotating coordinate system, which transforms the fifth and seventh harmonics into direct variables by distracting them through a low-pass filter and then achieves astatic control by the PI controller. Liu *et al.* [8] proposed a resonant control strategy to suppress the stator harmonic current of the DFIG. Zmood and Holmes [9] introduced the principle of the resonant controller in detail and revealed the equivalent conversion relationship between the proportional resonant (PR) and PI controller. Due to its effective controlling performance of alternating variables, lots of extensive researches around it have been proceeding. Yepes *et al.* [10] carried out an overall performance comparative analysis of several discretization methods of PR, providing a base of its engineering application; Vidal *et al.* [11] presented a parameter tuning and optimization method of PR considering transient response property of the controller. Meanwhile, different application forms of resonant control have be explored, e.g., the proportional integral resonant (PIR) controller in [12]–[14] and the vector proportional integral (VPI) controller under the synchronous rotating reference frame in [15] and [16]. They take the advantage of bidirectional resonance of the resonant controller to reduce the necessary controller numbers and there exists equivalent conversion relationship between PR, PIR, and VPI from the viewpoint of basic principle. The above mentioned strategy manifests excellent performance in case study; nonetheless, there remain several main drawbacks in the resonant-based strategy. For one controller could regulate at most two orders of harmonic components, the required number of the resonant controller is infinite in theory under real power grid circumstances where many kinds of harmonic voltage components besides fraction times of the fundamental frequency exist, and it should also be highlighted that several resonant controllers could pose a big difficulty on the digital computation resources. Recently, based still on the basic principle of the resonant controller, the authors of [17]–[20] presented a sort of repetitive controller (RC) and [21] proposed a sort of RC even with adaptability to minute changes of the grid voltage frequency to decrease the required number effectively, which is still a relief on controller number difficulty rather than a thorough solution. The instantaneous and accurate detection of harmonic components of the grid voltage is indispensable in such strategies, which is still a challenge at present.

Due to the shortage in traditional control strategy, it is a worthwhile attempt to introduce other nonlinear control strategies with effective regulating ability of alternating variables to DFIG. Since the time Germany scholar Blaschke proposed VC in 1972 [22], it has stepped into a revolutionary stage in the field of motor control; the following direct torque control (DTC) proposed by Depenbrock in 1988 [23] was another milestone in this realm. However, the complicated coordinate conversion and rigorous field orientation needed in VC have constrained its engineering application; the look-up table DTC has an unsatisfied steady performance due to the adoption of hysteresis control even if it has better dynamic performance and is easier to push into engineering application than VC. These two strategies are put into DFIG control application in [24] and [25] derivatively and have the above characteristics. In 1991, Kanellako *et al.* presented a nonlinear feedback controlling design method-backstepping algorithm at first [26], which has attracted much attention due to its excellent performance and huge potential in dealing with nonlinear systems. Considering its decoupling control capacity of nonlinear systems and no PI controller whose bandwidth limits its modulation of alternating variables, the backstepping algorithm is adaptive to be adopted in a strong coupling nonlinear DFIG system which concludes many alternating modulating components under harmonic grid voltage situation. Meanwhile, the development direction of control strategy in recent years tends to DPC and improvement of power quality [27], [28], which is taken into account in this paper as well.

This paper develops a backstepping-based DPC (BS-DPC) to DFIG under normal and harmonic grid voltage situations, which adopt space-vector pulse width modulation (SVPWM) in the last step to achieve the fixed switching frequency. First, the power model of the DFIG under the harmonic grid voltage is founded and power control objectives are devised in Section II-A; in the following Section II-B, the detailed mathematic model of the DFIG under the harmonic grid voltage is depicted; the backstepping algorithm is described briefly and the final BS-DPC of DFIG could be obtained based on above analysis in Section II-C. It should be stated that the normal grid voltage could be considered as a special situation of the harmonic voltage. Second, the proposed strategy is verified by the case simulation besides VC with the resonant controller in [8], the look-up table DPC (LUT-DPC) in [26] with improved control objectives proposed by this paper, and BS-DPC under normal and distorted grid voltage in Section III. Finally, systematic conclusions could be gained in Section IV on the above analysis and validation.

## II. Unified Backstepping-Based DPC Design of the DFIG

In this paper, the entire design process of BS-DPC of the DFIG is divided into three steps including the unified control objective design, the establishment of the unified DFIG mathematic model, and the final BS-DPC design under the normal and harmonic grid voltage. The unified control objective design is essential, thus being the first step.

### A. Power Control Objectives Design

In the stationary two-phase coordinate system, the apparent power poured into the grid through the stator of the DFIG could

be expressed as

$$\boldsymbol{S} = \frac{3}{2}\boldsymbol{U}_{s\alpha\beta}\boldsymbol{I}^{\wedge}_{s\alpha\beta} \tag{1}$$

where constant amplitude coordinate transformation is adopted.

Under the normal grid voltage, $\boldsymbol{U}_{S\alpha\beta}$ and $I_{S\alpha\beta}$ only comprise alternating components of the fundamental frequency which could generate constant active and reactive power; however, there would exist many different frequency voltage components under the harmonic grid voltage, which would induce the stator harmonic current and corresponding stator power fluctuation, unless improved control algorithm and power control objectives are adopted. Under any situation, the grid voltage and the stator current could be decomposed and expressed as

$$\boldsymbol{U}_{S\alpha\beta} = \boldsymbol{U}_{S\alpha\beta\_f} + \sum \boldsymbol{U}_{S\alpha\beta\_h} \tag{2a}$$

$$I_{S\alpha\beta} = I_{S\alpha\beta\_f} + \sum I_{S\alpha\beta\_h} \tag{2b}$$

where $\boldsymbol{U}_{S\alpha\beta\_f}, \boldsymbol{I}_{S\alpha\beta\_f}$ and $\sum \boldsymbol{U}_{S\alpha\beta\_h}, \sum \boldsymbol{I}_{S\alpha\beta\_h}$ represent the fundamental frequency and the harmonic components of the grid voltage and the stator current, respectively. In order to eliminate the stator harmonic current poured into the grid, power control targets should be set at first. Supposing that the control strategy is effective, the stator harmonic current would be equal to zero and the power targets could be obtained as

$$\boldsymbol{S} = \frac{3}{2}\boldsymbol{U}_{S\alpha\beta\_f}\boldsymbol{I}^{\wedge}_{s\alpha\beta\_f} + \frac{3}{2}\sum \boldsymbol{U}_{S\alpha\beta\_h}\boldsymbol{I}^{\wedge}_{s\alpha\beta\_f} \tag{3}$$

where the first item is the apparent power of principal power control targets $P^{*}_{S_\mathrm{main}}$and $Q^{*}_{S\_\mathrm{main}}$ which are equal to the given ones under the normal grid voltage, while the second is the compensation item under the distorted voltage. Decoupling the apparent compensation power, the following compensation control objectives can be gained:

$$\begin{cases} P^{*}_{S\_\mathrm{comp}} = \dfrac{3}{2}\sum \boldsymbol{U}_{S\alpha\_h}\boldsymbol{I}_{S\alpha\_f} + \dfrac{3}{2}\sum \boldsymbol{U}_{S\beta\_h}\boldsymbol{I}_{S\beta\_f} \\ Q^{*}_{S\_\mathrm{comp}} = \dfrac{3}{2}\sum \boldsymbol{U}_{S\beta\_h}\boldsymbol{I}_{S\alpha\_f} - \dfrac{3}{2}\sum \boldsymbol{U}_{S\alpha\_h}\boldsymbol{I}_{S\beta\_f}. \end{cases} \tag{4}$$

Fundamental frequency components always have a fixed frequency with very minute fluctuation; therefore, it is easy to decompose the grid voltage as (2) using fundamental frequency notch filters. Then, the calculation module of the compensation power could be depicted in Fig. 1.

It is necessary to find an algorithm which could regulate direct and alternating variables effectively but with excellent performance.

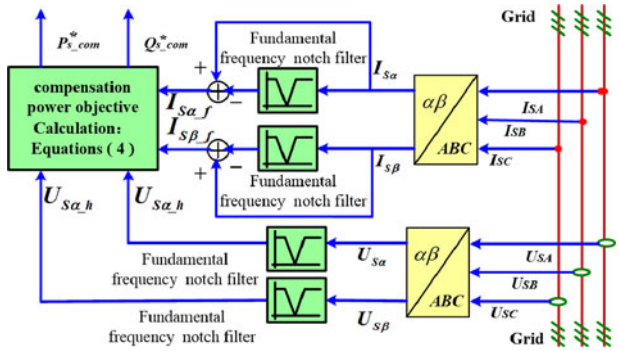


Fig. 1. Block diagram of the proposed improved compensation power control objective calculation.

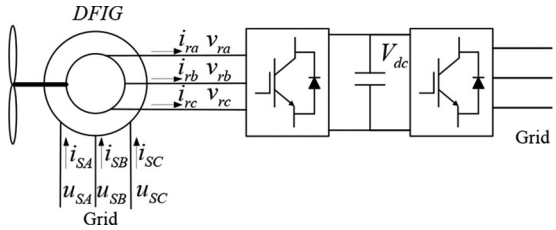


Fig. 2. Schematic diagram of the wind turbines-driven DFIG.

### B. Establishment of the DFIG Model

A typical layout of a wind turbine-driven DFIG is shown in Fig. 2 in which the voltage and current direction standard of the DFIG stator and rotor adopts the customary rule of the electric motor. Namely, the winding current direction is consistent with their direction of the voltage drop.

Through constant amplitude coordinate transformation, in the static $\alpha\beta$ coordinate system, the voltage of the DFIG could be expressed as

$$\begin{cases} \boldsymbol{U}_{s\alpha\beta} = R_s\boldsymbol{I}_{s\alpha\beta} + \frac{d\boldsymbol{\psi}_{s\alpha\beta}}{dt} \\ \boldsymbol{V}_{r\alpha\beta} = R_r\boldsymbol{I}_{r\alpha\beta} + \frac{d\boldsymbol{\psi}_{r\alpha\beta}}{dt} - j\omega_r\boldsymbol{\psi}_{r\alpha\beta} \end{cases} \tag{5}$$

and flux equations as

$$\begin{cases} \boldsymbol{\psi}_{s\alpha\beta} = L_s\boldsymbol{I}_{s\alpha\beta} + L_m\boldsymbol{I}_{r\alpha\beta} \\ \boldsymbol{\psi}_{r\alpha\beta} = L_r\boldsymbol{I}_{r\alpha\beta} + L_m\boldsymbol{I}_{s\alpha\beta}. \end{cases} \tag{6a}$$

$$\begin{cases} \boldsymbol{\psi}_{r\alpha\beta} = \sigma L_m\boldsymbol{I}_{s\alpha\beta} + \frac{L_r}{L_m}\boldsymbol{\psi}_{s\alpha\beta} \\ \boldsymbol{\psi}_{s\alpha\beta} = \sigma L_m\boldsymbol{I}_{r\alpha\beta} + \frac{L_s}{L_m}\boldsymbol{\psi}_{r\alpha\beta} \end{cases} \tag{6b}$$

where $\sigma = 1 - L_sL_r/L_m^2$ is the leakage factor.

From (5) and (6b), the following could be deduced: equation (7) is shown at the bottom of the page.

$$\begin{cases} \frac{d\boldsymbol{I}_{s\alpha\beta}}{dt} = \frac{1}{\sigma L_m}\left[(\boldsymbol{V}_{r\alpha\beta} - R_r\boldsymbol{I}_{r\alpha\beta}) - \frac{L_r}{L_m}(\boldsymbol{U}_{s\alpha\beta} - R_s\boldsymbol{I}_{s\alpha\beta}) + j\omega_r(\sigma L_m\boldsymbol{I}_{s\alpha\beta} + \frac{L_r}{L_m}\boldsymbol{\psi}_{s\alpha\beta})\right] \\ \frac{d\boldsymbol{I}_{r\alpha\beta}}{dt} = \frac{1}{\sigma L_m}\left[(\boldsymbol{U}_{s\alpha\beta} - R_s\boldsymbol{I}_{s\alpha\beta}) - \frac{L_s}{L_m}(\boldsymbol{V}_{r\alpha\beta} - R_r\boldsymbol{I}_{r\alpha\beta}) - j\frac{\omega_r L_s}{L_m}(\sigma L_m\boldsymbol{I}_{s\alpha\beta} + \frac{L_r}{L_m}\boldsymbol{\psi}_{s\alpha\beta})\right] \end{cases} \tag{7}$$

Differentiate equation (1) as follows:

$$\frac{d\boldsymbol{S}}{dt}=\frac{3}{2}\left(\boldsymbol{U}_{s\alpha\beta}\frac{d\boldsymbol{I}^{\wedge}_{s\alpha\beta}}{dt}+\boldsymbol{I}^{\wedge}_{s\alpha\beta}\frac{d\boldsymbol{U}_{s\alpha\beta}}{dt}\right). \tag{8}$$

Under harmonic grid voltage situation, the time derivative of the stator voltage of the DFIG could be deduced as

$$\frac{d\boldsymbol{U}_{s\alpha\beta}}{dt}=j\omega_f\boldsymbol{U}_{s\alpha\beta\_f}+\sum j\omega_h\boldsymbol{U}_{s\alpha\beta\_h}. \tag{9}$$

Defining $u_1=\sum j\left(\omega_h-\omega_f\right)\boldsymbol{U}_{S\alpha\beta\_h}$, then, the above equation could be rewritten as

$$\frac{d\boldsymbol{U}_{s\alpha\beta}}{dt}=j\omega_f\boldsymbol{U}_{s\alpha\beta}+u_1. \tag{10}$$

Substitute (7) and (10) into (8) and simplify the equation as

$$\begin{aligned}\frac{d\boldsymbol{S}}{dt}=&\frac{3}{2\sigma L_m}\left[\begin{array}{l}\boldsymbol{U}_{s\alpha\beta}\boldsymbol{V}^{\wedge}_{r\alpha\beta}-j\dfrac{L_r\omega_r}{L_m}\boldsymbol{U}_{s\alpha\beta}\boldsymbol{\psi}^{\wedge}_{s\alpha\beta}\\+\left(\dfrac{2L_rR_s}{3L_m}\boldsymbol{S}-R_r\boldsymbol{U}_{s\alpha\beta}\boldsymbol{I}^{\wedge}_{r\alpha\beta}\right)-\dfrac{L_r}{L_m}\left|\boldsymbol{U}_s\right|^2\end{array}\right]\\&+j\omega_f\boldsymbol{S}+\boldsymbol{I}^{\wedge}_{r\alpha\beta}u_1\end{aligned} \tag{11}$$

where $\omega_{\text{slip}}=\omega_f-\omega_r$ is the slip angular frequency of the DFIG.

Ignoring the impact of the stator resistance on the stator flux, the following could be obtained:

$$\boldsymbol{\psi}_{s\alpha\beta}=-j\frac{1}{\omega_f}\boldsymbol{U}_{s\alpha\beta\_f}-\sum j\frac{1}{\omega_h}\boldsymbol{U}_{s\alpha\beta\_h}. \tag{12}$$

If defining $u_2=\sum j\left(\frac{1}{\omega_f}-\frac{1}{\omega_h}\right)\boldsymbol{U}_{s\alpha\beta\_h}$, then, (12) could be rewritten as

$$\boldsymbol{\psi}_{s\alpha\beta}=-j\frac{1}{\omega_f}\boldsymbol{U}_{s\alpha\beta}+u_2. \tag{13}$$

Substituting (13) into (11), gain the following:

$$\begin{aligned}\frac{d\boldsymbol{S}}{dt}=&\frac{3}{2\sigma L_m}\left(\begin{array}{l}\boldsymbol{U}_{s\alpha\beta}\boldsymbol{V}^{\wedge}_{r\alpha\beta}-\dfrac{L_r}{L_m}\dfrac{\omega_{slip}}{\omega_f}\left|\boldsymbol{U}_s\right|^2\\-R_r\boldsymbol{U}_{s\alpha\beta}\boldsymbol{I}^{\wedge}_{r\alpha\beta}-j\dfrac{L_r\omega_r}{L_m}\boldsymbol{U}_{s\alpha\beta}u^{\wedge}_2\end{array}\right)\\&+j\omega_f\boldsymbol{S}+\boldsymbol{I}_{r\hat{\alpha}\beta}u_1.\end{aligned} \tag{14}$$

Under normal grid voltage situation, $u_1$ and $u_2$ are equal to zero; under the distorted grid voltage, the distorted degree is so low in general that $u_1$ is very close to zero and comparing with other items, the items concluding $u_2$ are small enough to be neglected, which is also under the consideration of eliminating the need of instantaneous detection of the harmonic grid voltage to provide conveniences of engineering application. Then, decoupling the apparent power, the active and reactive power could be expressed as

$$\left\{\begin{array}{l}\frac{dP_s}{dt}=-\dfrac{3}{2\sigma L_m}\dfrac{L_r}{L_m}\dfrac{\omega_{\text{slip}}}{\omega_f}\left|\boldsymbol{U}_s\right|^2-\omega_{\text{slip}}Q_s+\dfrac{L_r}{\sigma L_m}\dfrac{R_s}{L_m}P_S+\\\qquad\dfrac{3}{2\sigma L_m}\left(u_{s\alpha}v_{r\alpha}+u_{s\beta}v_{r\beta}\right)-\dfrac{3R_r}{2\sigma L_m}\left(u_{s\alpha}i_{r\alpha}+u_{s\beta}i_{r\beta}\right)\\\dfrac{dQ_s}{dt}=\omega_{\text{slip}}P_s+\dfrac{3}{2\sigma L_m}\left(u_{s\beta}v_{r\alpha}-u_{s\alpha}v_{r\beta}\right)+\dfrac{L_r}{\sigma L_m}\dfrac{R_s}{L_m}Q_S-\\\qquad\dfrac{3R_r}{2\sigma L_m}\left(u_{s\beta}i_{r\alpha}-u_{s\alpha}i_{r\beta}\right).\end{array}\right. \tag{15}$$

### C. BS-DPC Design of the DFIG

Kokotovic is the first person who proposed the backstepping algorithm in 1991, which enables entire system to obtain overall and asymptotic stabilization if only each Lyapunov function is constructed to converge according to Lyapunov stability theory. The basic method is to decompose the complicated nonlinear system into several lower order subsystems no more than system orders, and then begin to design Lyapunov function from the lowest subsystem back until to the entire system step by step; among the process, intermediary virtue control variables have often been employed. Since the Lyapunov function construction of each step satisfies the general conditions for Lyapunov stability, the system could be guaranteed strictly stable.

Combining backstepping algorithm with DPC technique, this paper proposes a BS-DPC strategy of the DFIG whose target is to ensure the active and reactive power to chase the given values with no derivation. Thus, defining the derivation of them as

$$\left\{\begin{array}{l}e_p=P^*_s-P_s\\e_q=Q^*_s-Q_s\end{array}\right. \tag{16}$$

if $e_p$ and $e_q$ tend to zero, the control task would be achieved. Thus, choose $e_p$ and $e_q$ as state variable to construct Lyapunov function of system as

$$V=\frac{1}{2}e_p^2+\frac{1}{2}e_q^2. \tag{17}$$

In general, the DFIG operates at a relatively smooth variation state, meaning that the given main control objective values of active and reactive powers could be seemed to remain constant; therefore, their differential coefficient could be considered equal to zero approximately. Doing derivation with (17), the following could be gained:

$$\begin{aligned}\frac{dV}{dt}=&\ e_p\frac{de_p}{dt}+e_q\frac{de_q}{dt}\\=&\ -e_p\left\{\begin{array}{l}-\dfrac{3}{2\sigma L_m}\dfrac{L_r}{L_m}\dfrac{\omega_s}{\omega_f}\left|\boldsymbol{U}_s\right|^2-\omega_{\text{slip}}Q_s-\dfrac{dP^*_{S\_\text{com}}}{dt}\\\dfrac{3}{2\sigma L_m}\left(u_{s\alpha}v_{r\alpha}+u_{s\beta}v_{r\beta}\right)-\dfrac{3R_r}{2\sigma L_m}\\\qquad\left(u_{s\alpha}i_{r\alpha}+u_{s\beta}i_{r\beta}\right)\end{array}\right\}\\&-e_q\left[\begin{array}{l}\omega_{\text{slip}}P_s+\dfrac{3}{2\sigma L_m}\left(u_{s\beta}v_{r\alpha}-u_{s\alpha}v_{r\beta}\right)-\\\dfrac{3R_r}{2\sigma L_m}\left(u_{s\beta}i_{r\alpha}-u_{s\alpha}i_{r\beta}\right)-\dfrac{dQ^*_{S\_\text{com}}}{dt}\end{array}\right].\end{aligned} \tag{18}$$

It could be deduced from the Lyapunov stability principle that when $V > 0$ and $dV/dt < 0$, the system would tend to stabilize. Thus, construct the following relational expression:

$$\begin{cases} k_p e_p = -\dfrac{3}{2\sigma L_m}\dfrac{L_r}{L_m}\dfrac{\omega_s}{\omega_f}\left|\boldsymbol{U}_s\right|^2 - \omega_{\text{slip}} Q_s - \dfrac{dP^*_{S\_\text{com}}}{dt} + \\ \qquad \dfrac{3}{2\sigma L_m}\left(u_{s\alpha} v_{r\alpha} + u_{s\beta} v_{r\beta}\right) - \dfrac{3R_r}{2\sigma L_m}\left(u_{s\alpha} i_{r\alpha} + u_{s\beta} i_{r\beta}\right) \\ k_q e_q = \omega_{\text{slip}} P_s + \dfrac{3}{2\sigma L_m}\left(u_{s\beta} v_{r\alpha} - u_{s\alpha} v_{r\beta}\right) - \\ \qquad \dfrac{3R_r}{2\sigma L_m}\left(u_{s\beta} i_{r\alpha} - u_{s\alpha} i_{r\beta}\right) - \dfrac{dQ^*_{S\_\text{com}}}{dt}. \end{cases} \tag{19}$$

Substituting (19) into (18), gain the following:

$$\frac{dV}{dt} = -k_p e_p^2 - k_q e_q^2 \tag{20}$$

where $k_p$ and $k_q$ act as the modulating coefficient of the active and reactive power, respectively. As long as $k_p > 0$ and $k_q > 0$ are set, $dV/dt < 0$ could be obtained; meanwhile, $V > 0$ could be deduced from (17) with ease. Thus, the stability of the DFIG system has been guaranteed.

Do integration with $dV/dt \le 0$ as

$$\int_0^\infty (dV/dt)dt = V(\infty) - V(0) \le 0. \tag{21}$$

It could be deduced from (17) that $V(\infty) \ge 0$, thus gaining the following:

$$-V(0) \le V(\infty) - V(0) \le 0. \tag{22}$$

Therefore, it could be known that the integration $\int_0^\infty (dV/dt)\,dt$ exists and has a certain bound; according to Barbalat theorem in [29], the equation $\lim_{t\to\infty} dV/dT = 0$ could be deduced; considering (20), then, further $\lim_{t\to\infty} e_p = 0$ and $\lim_{t\to\infty} e_q = 0$ could be obtained. In conclusion, the backstepping algorithm could achieve the accurate chase of given value with zero derivation.

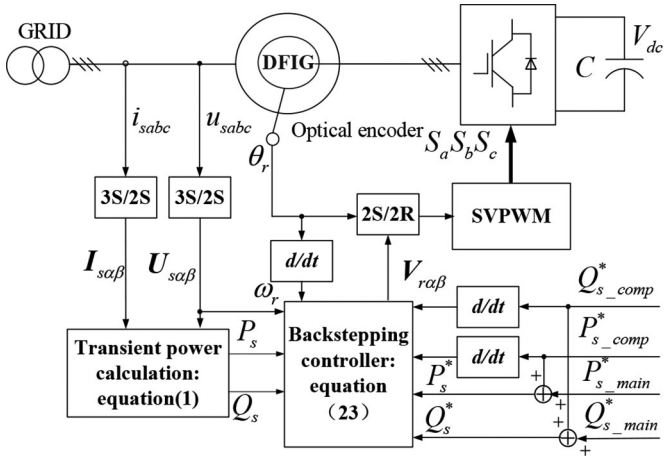


Fig. 3. Block diagram of BS-DPC for wind turbines-driven DFIG.

Solving (19), the modulating input voltage value needed by SVM of the DFIG rotor-side converter under the stationary two-phase coordinate system could be gained as (23) is shown at the bottom of the page.

Based on the above detailed analysis and design, the control scheme of BS-DPC strategy applying in a DFIG system under normal and harmonic grid voltage situation could be described in Fig. 3. The measured three-phase stator voltage and currents are directly transformed into the stationary two-phase coordinate system, which could be utilized to calculate the instantaneous active and reactive power by (1); the given power values $P^*_S$ and $Q^*_S$ including main and compensation targets, together with the above gained $P_S$, $Q_S$, $U_{S\alpha\beta}$ and $I_{S\alpha\beta}$, as well as the differential coefficient of $P^*_{S\_\text{comp}}$ and $Q^*_{S\_\text{comp}}$, are all inputted into the BS-DPC controller using (23) to calculate the output reference voltage values under the stationary two-phase coordinate system; after transforming from stator reference to rotor reference coordinate of the DFIG rotor, it acts as input values of SVM module to produce the switching signal of rotor-side converter legs: $\boldsymbol{S}_\text{a}$, $\boldsymbol{S}_\text{b}$, and $\boldsymbol{S}_\text{c}$. The only two adjusting coefficients $k_p$ and

$$\begin{cases} v_{r\alpha} = \dfrac{2\sigma L_m}{3\left|U_s\right|^2}\begin{bmatrix} k_p u_{s\alpha}(P^*_s - P_s) - \dfrac{L_r R_s P_s}{\sigma L_m^2} \\ +k_q u_{s\beta}(Q^*_s - Q_s) - \dfrac{L_r R_s Q_s}{\sigma L_m^2} \\ +\omega_{\text{slip}} u_{s\alpha} Q_s + u_{s\alpha}\dfrac{dP^*_{s\_\text{comp}}}{dt} \\ -\omega_{\text{slip}} u_{s\beta} P_s + u_{s\beta}\dfrac{dQ^*_{s\_\text{comp}}}{dt} \end{bmatrix} + R_r I_{r\alpha} + \dfrac{L_r \omega_{\text{slip}}}{L_m \omega_f} u_{s\alpha} \\ v_{r\beta} = \dfrac{2\sigma L_m}{3\left|U_s\right|^2}\begin{bmatrix} k_p u_{s\beta}(P^*_s - P_s) - \dfrac{L_r R_s P_s}{\sigma L_m^2} \\ -k_q u_{s\alpha}(Q^*_s - Q_s) - \dfrac{L_r R_s Q_s}{\sigma L_m^2} \\ +\omega_{\text{slip}} u_{s\beta} Q_s + u_{s\beta}\dfrac{dP^*_{s\_\text{comp}}}{dt} \\ +\omega_{\text{slip}} u_{s\alpha} P_s - u_{s\alpha}\dfrac{dQ^*_{s\_\text{comp}}}{dt} \end{bmatrix} + R_r I_{r\beta} + \dfrac{L_r \omega_{slip}}{L_m \omega_f} u_{s\beta} \end{cases} \tag{23}$$

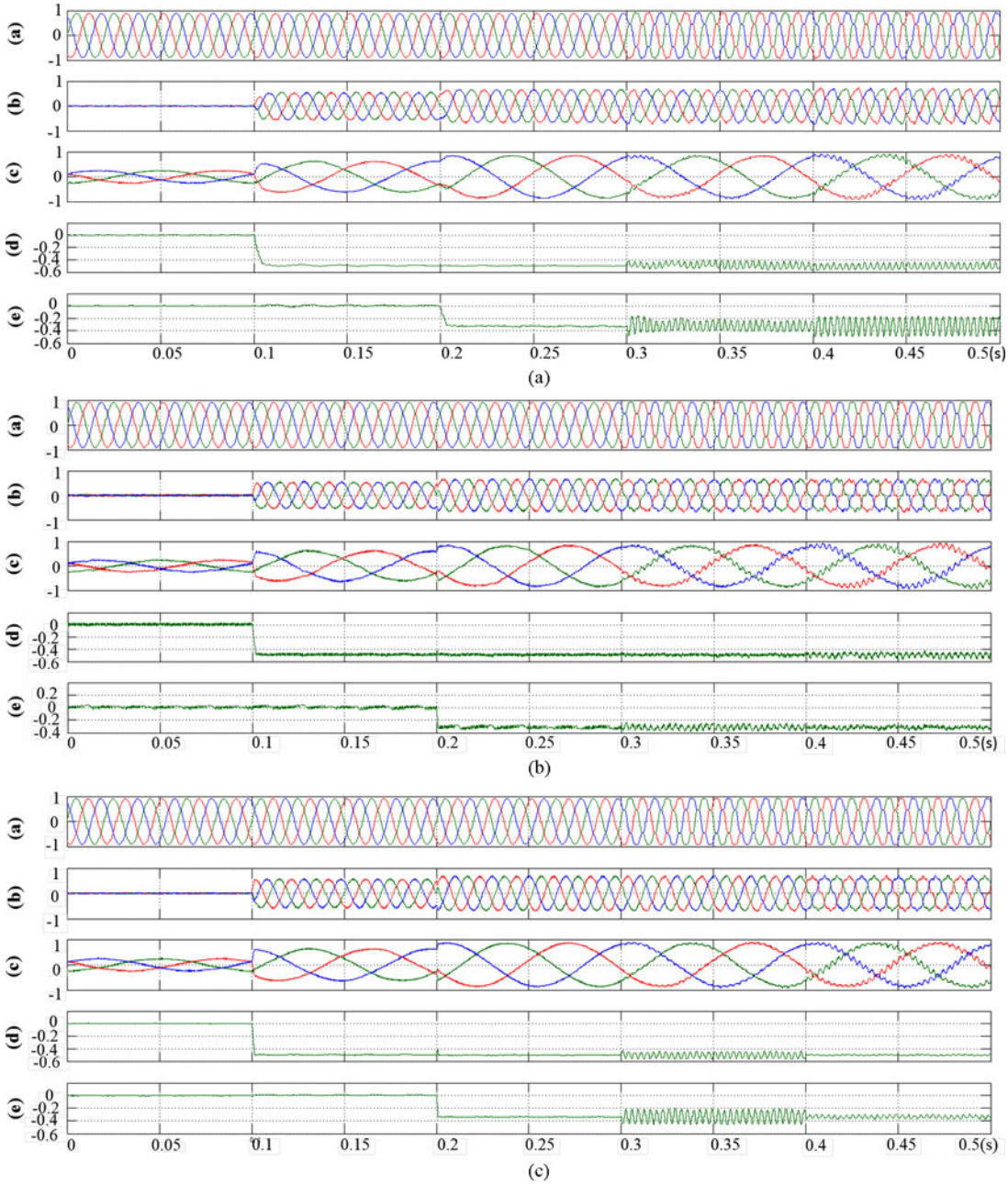


Fig. 4. Simulated results of VC with an additional resonant controller, LUT-DPC with improved power objectives proposed by this paper, and BS-DPC under the normal and harmonic grid voltage. (a) Three-phase stator voltages (in p.u.). (b) Three-phase stator currents (in p.u.). (c) Three-phase rotor currents (in p.u.). (d) Stator active power (in p.u.). (e) Stator reactive power (in p.u.). (A) STR. A: VC with additional resonant controller [8]. (B) STR. B: LUT-DPC [26] with improved power objectives proposed by this paper. (C) STR. C: Proposed BS-DPC.

$k_q$ required in proposed BS-DPC strategy give big advantages in engineering implementation, in contrast to five adjusting parameters of strategy proposed in [8]. Furthermore, together with the sufficient decoupling control of $k_p$ with active power and $k_q$ with reactive power, it is very simple of the coefficient adjusting regulation of BS-DPC that the dynamic performance is improved with the increasing of power adjusting coefficients, while the steady performance is improved with the decreasing of power adjusting coefficients, leading coefficient adjustment to just making a compromise between transient and steady performance of the DFIG. Meanwhile, as Fig. 3 shows, not only does BS-DPC require the similar amount of coordinate transforming calculation to the DPC proposed by [6], but also the control scheme of BS-DPC strategy is very concise.

## III. Simulation Results Analysis and Verification

Simulation researches based on MATLAB/Simulink have been conducted on a 2-MW wind turbine-driven DFIG to verify the proposed BS-DPC strategy under the normal and harmonic grid voltage. The system parameters are described in the Appendix. For the purpose of contrast analysis, the traditional VC

TABLE I
PERFORMANCE ANALYSIS OF SIMULATION RESULTS

| | Normal grid voltage conditions | | | | | Harmonic grid voltage conditions | | | | | |
|---|---|---|---|---|---|---|---|---|---|---|---|
| time | 0∼0.3S | | | | | 0.3∼0.4S | | | 0.4∼0.5S | | |
| Performance items | $P_S$ step response time (S) | $Q_S$ step response time (S) | $P_S$ pulsation (p.u.) | $Q_S$ pulsation (p.u.) | $I_{SA}$ THD (%) | $P_S$ pulsation (p.u.) | $Q_S$ pulsation (p.u.) | $I_{SA}$ THD (%) | $P_S$ pulsation (p.u.) | $Q_S$ pulsation (p.u.) | $I_{SA}$ THD (%) |
| STR. A | 0.005 | 0.004 | ±0.003 | ±0.003 | 0.87 | ±0.03 | ±0.042 | 2.1 | ±0.017 | ±0.083 | 9.3 |
| STR. B | 0.0022 | 0.0009 | ±0.025 | ±0.025 | 2.45 | ±0.033 | ±0.07 | 9.4 | ±0.063 | ±0.05 | 12.55 |
| STR. C | 0.0015 | 0.0008 | ±0.005 | ±0.005 | 1.61 | ±0.067 | ±0.117 | 3.31 | ±0.017 | ±0.037 | 10.97 |

STR.A: VC with additional resonant controller [7]; STR.B: LUT-DPC [21] with improved power objectives; STR.C: Proposed BS-DPC.

with an additional resonant controller proposed by [8] (STR. A), the traditional LUT-DPC by [26] with improved compensation power control objectives proposed by this paper (STR. B), and BS-DPC proposed by this paper (STR. C) have been tested under the same operating circumstance. In the first 0.3 s, the DFIGs are operating under the normal grid voltage, while during 0.3–0.5 s, they are operating under harmonic grid voltage condition, but from the time of 0.4 s on, the additional resonant controller of VC and the improved compensation control objectives of LUT-DPC and BS-DPC are shut down. Under the normal grid voltage, the reference value of the active power is given a step from 0 to $-0.5$ p.u. at 0.1 s, while the one of the reactive power is given a step from 0 to $-0.35$ p.u. at 0.2 s; afterward, the reference value of active and reactive remain unchanged in all the following simulations including under the harmonic grid voltage with 10% of negative sequence fifth order and 8% of seventh-order harmonics. The simulation results of the proposed BS-DPC strategy with contrast to two other strategies under the normal and harmonic grid voltage can be observed from Fig. 4, and the performance analysis and comparison are also listed in Table I.

The adjusting coefficients of STR. A are: proportional coefficients $k_{pd} = k_{pq} = 5$, integral coefficients $k_{id} = k_{iq} = 100$, and resonant coefficient $k_r = 200$. The adjusting coefficients of STR. C are: active power coefficient $k_p = 53$ and reactive power coefficient $k_q = 53$.

### A. Simulation Results Analysis Under the Normal Grid Voltage

As Fig. 4 and Table I show, under the normal grid voltage, BS-DPC has steady performance close to VC, for they both adopt the SVPWM method at the last step which could enable the converter to obtain comparatively fixed switching frequency. The result of LUT-DPC has less satisfactory steady performance than the other two, with bigger active and reactive pulsation and slight power chasing the steady-state error due to the utilization of hysteresis control. The total harmonic distortion (THD) comparison analysis of the stator A-phase current also manifests that the current poured by LUT-DPC has more harmonic component than by the other two, VC and BS-DPC, whose THD of current are at similar level. Nonetheless, LUT-DPC has much faster step response speed than VC, and BS-DPC also manifests excellent dynamic performance close to LUT-DPC as simulation results show. Thus, it can be concluded from the performance comparison under the normal grid voltage that the BS-DPC not only inherits excellent dynamic performance from traditional DPC but also has excellent steady performance close to VC, such as less harmonic current, less power pulsation, and constant switching frequency, etc.; meanwhile, BS-DPC has no need of complicated coordinate transformation and rigorous flux orientation in VC strategy.

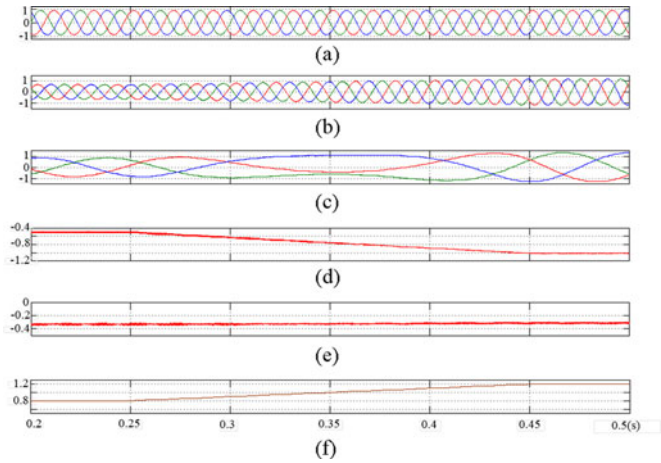


Fig. 5. Simulated results of BS-DPC adaptability to under variable wind speed. (a) Three-phase stator voltages (in p.u.). (b) Three-phase stator currents (in p.u.). (c) Three-phase rotor currents (in p.u.). (d) Stator active power (in p.u.). (e) Stator reactive power (in p.u.). (f) Generator speed (in p.u.).

The performance under the variable wind speed from subsynchronous to super-synchronous speed (from 0.8 p.u. at 0.25 s to 1.2 p.u. at 0.45 s), is verified under the normal grid voltage in Fig. 5. It should be stated that the relationship between the electromagnetic power and the rotor speed does not strictly accord with the aerodynamical relation for maximum power point tracking, for research of this paper is focused on electromagnetic relationship of the DFIG.

### B. Simulation Results Analysis Under the Harmonic Grid Voltage

The excellent dynamic and steady performance of BS-DPC under the normal grid voltage has founded the base to its further research under harmonic grid voltage conditions. After the grid voltage becomes distorted since 0.3 s, these three strategies, VC

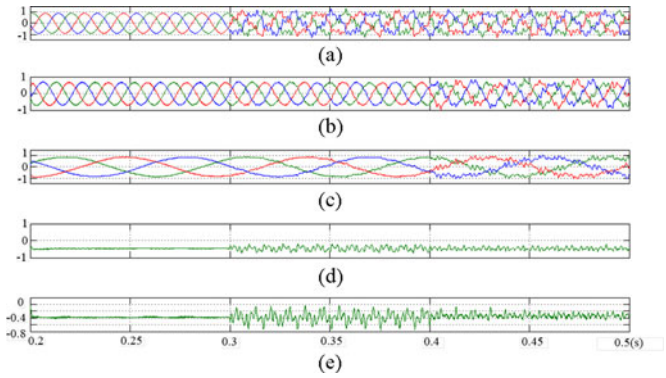


Fig. 6. Simulated results of BS-DPC adaptability to minute frequency change, distorted degree, and harmonic order of the grid voltage. (a) Three-phase stator voltages (in p.u.). (b) Three-phase stator currents (in p.u.). (c) Three-phase rotor currents (in p.u.). (d) Stator active power (in p.u.). (e) Stator reactive power (in p.u.).

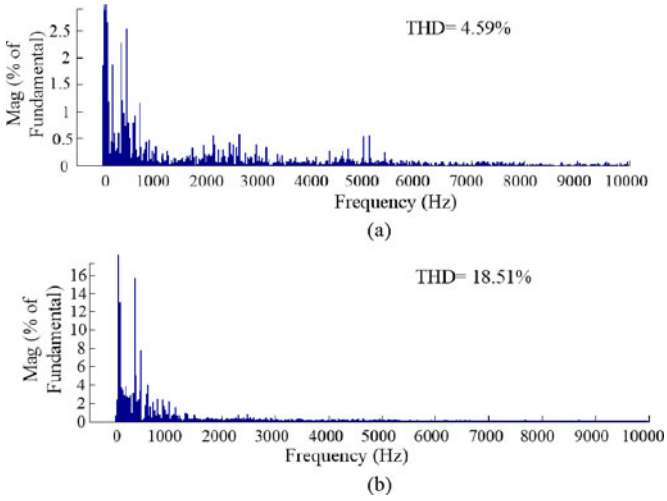


Fig. 7. Stator A phase current spectrum of BS-DPC adaptability to minute frequency change, distorted degree, and harmonic order of the grid voltage. (A) With harmonics suppression strategy (0.3–0.4 s). (B) Without harmonics suppression strategy (0.4–0.5 s).

with additional resonant controller, LUT-DPC with improved power objectives proposed by this paper, and BS-DPC, could all suppress the stator harmonic current effectively and by contrast, the stator current becomes seriously distorted after those three harmonic current suppression strategies are shut up since 0.4 s. Nevertheless, as Fig. 4 and Table I show, STR.C has manifested the rapid transient response speed evidently as soon as the grid voltage becomes distorted and steady effectiveness of stator harmonic current suppression close to STR.A, while STR. B has the worst steady harmonic current suppression performance even if it does have somewhat effectiveness, as well as STR. A has the most excellent steady performance and the worst transient response speed in harmonic current suppression. But in contrast to a resonant controller aiming at two typical orders harmonics suppression, it should also be highlighted that BS-DPC could operate with no typical order, magnitude, and number limits of harmonics, and has a certain adaptability of the grid voltage frequency as shown by the simulation results in Figs. 6 and 7.

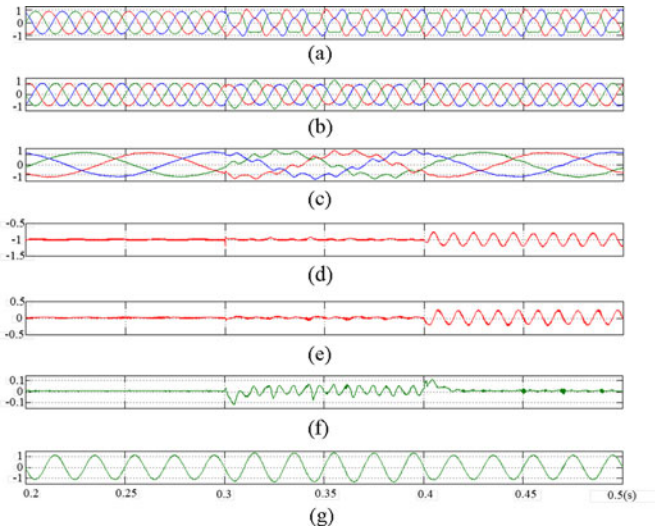


Fig. 8. Simulated results of BS-DPC at rated condition and the stability of system during the transient state under the presence of harmonics. (a) Three-phase stator voltages (in p.u.). (b) Three-phase stator currents (in p.u.). (c) Three-phase rotor currents (in p.u.). (d) Stator active power (in p.u.). (e) Stator reactive power (in p.u.). (f) Stator phase A harmonic current components (in p.u.). (g) Stator phase A fundamental frequency current component (in p.u.).

The adaptability simulation of BS-DPC in Fig. 6 is carried out under similar circumstance to above other than the grid voltage frequency of 51 Hz, and more arbitrary harmonic orders and bigger magnitude, 20% of the 3.3th, 20% of the 9.1th, 8% of the 13.7th, 5% of the −7th, 3% of the −9.1th, and 2% of the 17th-order harmonic voltage. It could be observed from Fig. 6 that the outputting stator current of the DFIG remains very sinusoidal when using harmonic suppression strategy; meanwhile, as Fig. 7 shows, corresponding harmonic current of 3.3th and 9.1th orders are suppressed sufficiently from 13% to 2.3% and from 16% to 2.7%, respectively. It should be noticed that the distorted degree and pulsation amplitude of the active and reactive power might be different as shown during 0.3–0.4 s in Fig. 6, which depends on the initial phase difference between the resultant vector of different frequency harmonic grid voltage and fundamental frequency current vector of the DFIG stator. Instantaneous and accurate detection of harmonic components and phase positions of the grid voltage would still pose a challenge for the engineering application at present especially under distorted grid voltage situation, which have not been adopted in the above test of BS-DPC and LUT-DPC.

The performance of the DFIG controlled by the new scheme at rated condition and the stability of system during the transient state under the presence of harmonics under rated conditions is verified in Fig. 8. During the first 0.1 s, the performance of the DFIG controlled by the new scheme at rated condition agrees with the performance in Fig. 4 under the normal grid voltage. Since 0.3 s on, the 20% of the third-order harmonic voltage which exists in the real grid more often has been added. As the simulation during the last 0.1 s shows that the harmonic current components of stator phase-A are decaying from large to small, and close to zero within 0.014 s after the proposed strategy

is added, means that the transient state under the presence of harmonics is stable.

## IV. Conclusion

This paper has presented a nonlinear backstepping DPC strategy of the wind turbine-driven DFIG operating under normal and harmonic grid voltage situations. Simulation research on a 2-MW DFIG wind power generation system validates the proposed control strategies and the following conclusions can be gained as well.

1) Under the distorted grid voltage, the active and reactive power produced by the DFIG include alternating components unavoidably; through detailed analysis of control objectives, this paper divides these power components into main control objectives equal to given reference values and compensation ones which depend on the voltage distorted degree, and develops a way to draw compensation control objectives. It should be highlighted that those control objectives are adaptive under the normal grid voltage, thus establishing the uniform calculating module of power objectives under the normal and harmonic grid voltage. This also could be adopted by some existing control strategy without PI controller (e.g., LUT-DPC, etc.), which has also been verified by simulation results.
2) As a nonlinear control design method, the backstepping algorithm could achieve decoupling control of the active and reactive power of the DFIG without any PI controller, leading to its potential to regulate alternating variables effectively. It could be concluded from the simulation results under the normal grid voltage that its operating performance is excellent with steady performance close to VC and with dynamic performance similar to LUT-DPC. In contrast to traditional VC, due to no complicated coordinate transformation and less adjusting parameters, the proposed backstepping algorithm is much easier to put into engineering application.
3) According to the simulation results under the harmonic grid voltage, the BS-DPC of the DFIG could achieve sufficient control of alternating components with stator harmonic current suppression performance similar to the resonant-based controller. However, it should be highlighted that one resonant controller could only operate under one or two typical harmonic orders with the help of accurate and instantaneous detection of grid voltage harmonic components, while the BS-DPC is carried out without any concrete harmonic order limit and phase detection. This helps to form a comprehensive control strategy under any distorted grid voltage condition rather than under particular harmonic orders, leading to its huge engineering application value. Although the grid circumstance may be different (under the normal and harmonic grid voltage, or different distorted degree grid voltage), the BS-DPC algorithm itself is the same set, so is the control objective calculations. This could also help to establish a uniform and comprehensive control algorithm of the DFIG. Its excellent adaptability to minute frequency change, distorted degree, and harmonic order of the grid voltage are verified by simulation results as well. Combining adaptive control with the backstepping algorithm to improve its robustness against system parameter turbulence is one research direction in future.

## Appendix

TABLE II
Parameters of the Simulation System

| | | | |
|---|---|---|---|
| Rated power | 2 MW | Rotor resistance | 0.1286 p.u. |
| Rated grid voltage | 690V | Stator resistance | 0.0959 p.u. |
| Rated frequency | 50 Hz | DFIG rotation rate | 0.8 p.u. |
| Pole number | 2 | DC-link voltage | 1200V |
| Stator/rotor turns ratio | 1.9485 | Mutual inductance | 3.6757 p.u. |
| Stator leakage inductance | 0.1169 p.u. | Rotor leakage inductance | 0.1169 p.u. |
| Convertor switching frequency | 2.5 KHz | LUT-DPC sampling frequency | 10 KHz |
| VC sampling frequency | 5 KHz | BS-DPC sampling frequency | 5 KHz |

## References


[1] Energinet. Dk. (2010, Sep.). Technical regulation 3.2.5 for wind power plants with a power output greater than 11kW. [Online]. Available: http://www.energinet.dk

[2] *Electromagnetic Compatibility (EMC)—Part 3–6: Assessment of Harmonic Emission Limits for the Connection of Distorting Installations to MV, HV EHV Power Systems*, IEC Standard IEC 61000-3-6 Ed.2, 2007.

[3] *IEEE Recommended Practices and Requirements for Harmonic Control in Electrical Power Systems*, IEEE Standard 519-1992, 1993.

[4] G. Hensman, "Connecting nonlinear loads to public electricity systems: A guide to engineering recommendation G5/4," *Power Eng. J.*, vol. 16, no. 2, pp. 77–87, Apr. 2002.

[5] J. B. Hu, H. L. Xu, and Y. K. He, "Coordinated control of DFIG's RSC and GSC under generalized unbalanced and distorted grid voltage conditions," *IEEE Trans. Ind. Electron.*, vol. 60, no. 7, pp. 2808–2819, Jul. 2013.

[6] P. Zhou, Y. K. He, and D. Sun, "Improved direct power control of a DFIG-based wind turbine during network unbalance," *IEEE Trans. Power Electron.*, vol. 24, no. 11, pp. 2465–2474, Nov. 2009.

[7] C. J. Ramos, A. P. Martins, and A. S. Carvalho, "Rotor current controller with voltage harmonics compensation for a DFIG operating under unbalanced and distorted stator voltage," in *Proc. IEEE 33rd Annu. Conf. Ind. Electron. Soc.*, 2007, pp. 1287–1292.

[8] C. Liu, F. Blaabjerg, W. Chen, and D. Xu, "Stator current harmonic control with resonant controller for doubly fed induction generator," *IEEE Trans. Power Electron.*, vol. 27, no. 7, pp. 3207–3220, Jul. 2012.

[9] D. N. Zmood and D. G. Holmes, "Stationary frame current regulation of PWM inverters with zero steady-state error," *IEEE Trans. Power Electron.*, vol. 18, no. 3, pp. 814–822, May 2003.

[10] A. G. Yepes, F. D. Freijedo, J. Doval-Gandoy, O. López, J. Malvar, and P. Fernandez-Comesaña, "Effects of discretization methods on the performance of resonant controllers," *IEEE Trans Power Electron.*, vol. 25, no. 7, pp. 1692–1712, Jan. 2010.

[11] A. Vidal, F. D. Freijedo, A. G. Yepes, P. Fernandez-Comesana, J. Malvar, O. Lopez, and J. Doval-Gandoy, "Assessment and optimization of the transient response of proportional-resonant current controllers for distributed power generation systems," *IEEE Trans. Ind. Electron.*, vol. 60, no. 4, pp. 1367–1383, Feb. 2012.

[12] J. B. Hu and Y. K. He, "Modeling and enhanced control of DFIG under unbalanced grid voltage conditions," *Electric Power Syst. Res.*, vol. 79, no. 2, pp. 273–281, Feb. 2009.

[13] J. B. Hu, Y. K. He, L. Xu, and B. W. Williams, "Improved control of DFIG systems during network unbalance using PI–R current regulators," *IEEE Trans Ind. Electron.*, vol. 56, no. 2, pp. 439–451, Oct. 2008.

[14] R. Bojoi, L. R. Limongi, D. Roiu, and A. Tenconi "Frequency-domain analysis of resonant current controllers for active power conditioners," in *Proc. IEEE 34th Annu. Conf. Ind. Electron.*, 2008, pp. 3141–3148.

[15] C. Lascu, L. Asiminoaei, I. Boldea, and F. Blaabjerg, "High performance current controller for selective harmonic compensation in active power

filters," *IEEE Trans. Power Electron.*, vol. 22, no. 5, pp. 1826–1835, Sep. 2007.
[16] H. Nian and Y. P. Song, "Direct power control of doubly fed induction generator under distorted grid voltage," *IEEE Trans Power Electron.*, vol. 29, no. 2, pp. 894–905, Feb. 2014.
[17] D. Chen, J. Zhang, and Z. Qian, "Research on fast transient and 6n $\pm$1 harmonics suppressing repetitive control scheme for three-phase grid-connected inverters," *IET Power Electron.*, vol. 6, no. 3, pp. 601–610, 2013.
[18] Y. Yang, K. Zhou, M. Cheng, and B. Zhang, "Phase compensation multi resonant control of CVCF PWM converters," *IEEE Trans. Power Electron.*, vol. 28, no. 8, pp. 3923–3930, Aug. 2013.
[19] W. Lu, K. Zhou, D. Wang, and M. Cheng, "A general parallel structure repetitive control scheme for multiphase DC–AC PWM converters," *IEEE Trans. Power Electron.*, vol. 28, no. 8, pp. 3980–3987, Aug. 2013.
[20] F. Wei, X. Zhang, D. M. Vilathgamuwa, S. S. Choi, and S. Wang, "Mitigation of distorted and unbalanced stator voltage of stand-alone doubly fed induction generators using repetitive control technique," *IET Electron Power Appl.*, vol. 7, no. 8, pp. 654–663, 2013.
[21] Y. P. Song and H. Nian, "Sinusoidal output current implementation of DFIG using repetitive control under generalized harmonic power grid with frequency deviation," *IEEE Trans. Power Electron.*, vol. 30, no. 12, pp. 6751–6762, Jan. 2015.
[22] F. Blaschke, "The principle of field-orientation as applied to the new transvector closed-loop control system for rotating-field machines," *Stemens Rev.*, vol. 34, pp. 217–220, 1972.
[23] M. Depenbrock, "Direct self-control (DSC) of inverter-fed machine," *IEEE Trans Power Electron.*, vol. 3, no. 4, pp. 420–429, Oct. 1988.
[24] R. Pena, J. C. Clare, and G. M. Asher, "Doubly fed induction generator using back-to-back PWM converters and its application to variable-speed wind-energy generation," in *Proc. IEE B.*, vol. 143, no. 3, pp. 231–241, May 1996.
[25] L. Xu and P. Cartwright, "Direct active and reactive power control of DFIG for wind energy generation," *IEEE Trans. Energy Convers.*, vol. 21, no. 3, pp. 750–758, Sep. 2006.
[26] P. I. Kanellako, P. V. Kokotovic, and A. S. Morse, "Systematic design of adaptive controllers for feedback linearizable systems," *IEEE Trans. Autom. Control*, vol. 36, no. 11, pp. 1241–1253, Nov. 1991.
[27] L. Shang and J. B. Hu, "Sliding-mode-based direct power control of grid-connected wind-turbine-driven doubly fed induction generators under unbalanced grid voltage conditions," *IEEE Trans. Energy Convers.*, vol. 27, no. 2, pp. 362–373, Jun. 2012.
[28] M. Liserre, R. Cárdenas, M. Molinas *et al.*, "Overview of Multi-MW Wind Turbines and Wind Parks" *IEEE Trans. Ind. Electron.*, vol. 58, no. 4, pp. 1081–1095, Apr. 2011.
[29] J. Slotine and W. Li, *Applied Nonlinear Control*. Englewood Cliffs, NJ, USA: Prentice Hall, 1991, pp. 122–126.

**Pinghua Xiong** was born in Fengcheng, China, in 1980. He received the B.Sc. degree from the College of Power and Energy, Northwestern Polytechnical University, Xi' an, China, in July 2003. He is currently working toward the M.E. degree at the College of Electrical Engineering, Zhejiang University, Hangzhou, China.

His current research interests include motor control with power electronics devices in renewable-energy conversion, particularly the control and operation of doubly fed induction generators for wind power generation.

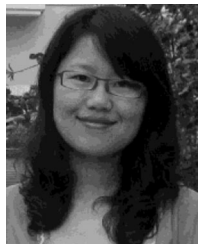

**Dan Sun** (M'05) received the B.E. degree from Shenyang Jianzhu University, Shenyang, China, the M.E. degree from Hohai University, Nanjing, China, and the Ph.D. degree from Zhejiang University, Hangzhou, China, in 1997, 2000, and 2004, respectively, all in electrical engineering.

In 2004, she joined the College of Electrical Engineering, Zhejiang University, where she has been an Associate Professor since 2007.

Her research interests include the advanced electric machine drives and control for the wind power generation system.